Journal of Materials Processing Tech. 291 (2021) 117050

Contents lists available at ScienceDirect

Journal of Materials Processing Tech.

journal homepage: www.elsevier.com/locate/jmatprotec

Characteristics of multiphase jet machining: A comparison with the absence of water

Yan Hu, Qingwen Dai, Wei Huang, Xiaolei Wang *

National Key Laboratory of Science and Technology on Helicopter Transmission, Nanjing University of Aeronautics & Astronautics, Nanjing, 210016, China

ARTICLE INFO

Associate Editor: A Clare

Keywords:
Abrasive air jet
Multiphase jet
Surface texture
Jet convergence
Water dedusting and lubrication

ABSTRACT

Multiphase jet machining (MJM) is a recently developed surface texturing method that introduces water into a dry abrasive air jet. However, there are still some unknown issues with MJM, especially regarding the effects of adding water. Hence, we conducted a series of comparative studies when water was added (wet conditions) or not (dry conditions). Dimples and masked channels were machined on Si wafer and cemented carbide (YG6) surfaces to quantify the machining profile, erosion rate and roughness. Numerical simulations and high-speed cameras were used to help understand the particle erosion mechanisms. It was found that the inhaled water was completely atomized to form droplets and wrapped the abrasive particles; thus, the abrasives tended to follow their original trajectories without being deflected by the divergent airflow. This convergent effect could reduce the jet diameter and thus improve the machining resolution. The machining footprint was found to be reduced by 47.2 % at a jet distance of 13 mm compared to without water. Experimental and numerical results confirmed that under wet conditions, most of the particles would flow close to the machined surface, thus introducing a sliding grinding effect. The net result was a decrease in erosion ability but an improvement in surface roughness. Particularly, for the machining of sintered materials, the roughness could be improved more than 2.5 times.

1. Introduction

Surface texture is beneficial for tribological purposes, triggering a new topic in manufacturing, i.e., surface texturing (Coblas et al., 2015). To ensure effects such as hydrodynamic pressure generation and lubricant reservoirs, the texture unit is usually shallow, typically from 0.5–50 μm in depth and 100 μm to millimeters in other dimensions on the surface of machine components (Yuan et al., 2011). The material to be processed also varies, from ductile materials, typically metals and alloys, to brittle materials such as glass and ceramics. The precision of the surface texturing techniques such as accuracy of the dimensions, geometric shape, control of edge angle, roughness of manufactured surface, and material property changes all constitute factors that will influence the tribological outcome. It is important to select manufacturing methods according to the specific application and material (Coblas et al., 2015).

Current techniques for surface texturing include laser machining (Schreck and Gahr, 2005), micromilling (Zhang, 2013), reactive ion etching (Wang and Kato, 2003); (Yu et al., 2013), electrical discharge machining (EDM), chemical wet etching and jet machining. Comparatively, jet machining technology has shown its application for surface texturing owing to the distinct features of machining hard and brittle materials without thermal damage and low operating costs. The traditional jets generally operate in a dry or wet format, as seen in Table 1, including the following: (1) abrasive air jet (AAJ); (2) water jet (WJ); (3) abrasive water jet (AWJ), including the modified high-pressure abrasive slurry jet (HASJ); and (4) abrasive slurry jet (ASJ). In the past few decades, these jet techniques have been developed to perform a wide variety of tasks due to their respective advantages. Generally, most WJs, AWJs and HASJs, including the modified PWJs (Lehocka et al., 2016), operate at very high pump pressures ranging from 200 to 600 MPa to achieve high jet velocities (up to 1000 m/s), so their high-pressure jet penetration or instantaneous impact force make them prominently used in application scenarios with bulk material removal effects such as material cutting, disintegration of coal, rock drilling, etc.

Low-pressure jet techniques such as ASJ and AAJ (typically 0–3 MPa), are usually used in processing where energy requirements are relatively low such as micromachining of blind/through holes and

* Corresponding author at: Yudao Street 29#, Nanjing, China.
E-mail address: wxl@nuaa.edu.cn (X. Wang).

https://doi.org/10.1016/j.jmatprotec.2021.117050
Received 31 October 2020; Received in revised form 3 January 2021; Accepted 11 January 2021
Available online 15 January 2021

Table 1
Literature results for various jet techniques.

	Type	Jet pressure (MPa)	Velocity (m/s)
Dry (air-based)	Abrasive air jet (AAJ)	0.1–0.6	100–200 (Luo et al., 2019)
Wet (water-based)	Water jet (WJ)	~600	~1078 (Maniadaki et al., 2007)
	Pulsating water jet (PWJ)	40	~200 (Lehocka et al., 2016)
	Abrasive slurry jet (ASJ)	0.5–3	15–89 (Kowsari et al., 2016), (Nouraei et al., 2013)
	High-pressure abrasive slurry jet (HASJ)	35	150–180 (Matsumura et al., 2011)
		134–263	200–400 (Haghbin et al., 2019)
	Abrasive water jet (AWJ)	100	250–450 (Zhang et al., 2017)

Table 2
Literature results for various wet AAJs.

Slurry entry	Nozzle exit type	Application
Fig. 1(c)	Cylinder (180 or 254 μm)	Unmasked hole or channel (Nouraei et al., 2013)
Fig. 1(d)	Square (3 mm × 3 mm)	Erosion of coating (Iwai et al., 2009)
Fig. 1(d)	Cylinder (3 or 4 mm)	Polishing (Tsai et al., 2008), (Yan et al., 2008)
Fig. 1(d)	Cylinder (6 mm)	Fracture-free texture (Mineta et al., 2009)
Fig. 1(d)	Cylinder (8 mm)	Surface modification (Freiburg et al., 2019)
Fig. 1(d)	Square (1 mm × 1 mm)	Wear test (Nakanishi et al., 2015, 2017, 2018); polishing (Baba et al., 2019)

channels on glass, turning, polishing, paint or scale removal, pretreatment of plating and painting, deburring, etc. One of the distinct features of AAJs is that it uses a cheap and low-pressure air pump of 0.1–0.6 MPa to achieve a relatively high velocity (100–200 m/s), which is significantly higher than the velocity range of the ASJs (15–89 m/s). Hawthorne et al. (1999) and Beaucamp et al. (2017) found that under the same working pressure, the material removal rate of AAJ is 3 times the material removal rate of ASJ because of the confirmation that the particle impact velocities in the air jet (84 m/s) are much higher than the particle impact velocities of the slurry jet (15 m/s). However, for ASJs, normal incidence with pressures of 0.5–3 MPa presents a "W"-shaped removal in the cross section, as noted by Cao and Cheung (2014); Cao et al. (2016). Thus, the ASJs will induce a mid-high spatial frequency residual even if complex tool path planning or oblique incidence from different positions are applied. Comparatively, AAJ is more conducive to the formation of planar or regular microstructures due to its rotational symmetrical Gaussian-like removal profile ("U"-shape) (Balasubramaniam et al., 2002).

However, AAJ is inconveniently carried out in the blasting chamber connected to a dust collector, and the operators normally wear particulate respirators. Using fine abrasives to reduce the size of machined features will lead to longer particle settling times, larger contaminated areas and difficult recovery of abrasives (Jafar et al., 2016). Use of precious abrasives is costly. Usually, dry abrasive particles used in traditional AAJs are characterized by high hardness and sharp corners. When high-speed particles (compared to ASJs) impact the surface, the pierce points of the substrate are deeper, resulting in a rough glass surface that has been reported to be as high as 8–10 μm for 30-μm diameter particles (Ghobeity et al., 2012). Beaucamp et al. (2017) and Ghobeity et al. (2012) indicated that the roughness of AAJ machined microchannels is generally larger than the roughness from other methods of micromachining such as ASJs and wet etching, which should be a critical issue in microfluidic applications. Another potential disadvantage of AAJs is that the compressed air jet diverges significantly after the nozzle exit, lowering the resolution of micromachined features (Luo et al., 2019).

Therefore, with the advantages of low pressure but high material removal rate and U-shaped erosion profile, methods to reduce the dust dispersion, roughness and size of the machining footprint resulting from dry AAJ operations are meaningful.

To ameliorate the abovementioned dilemmas, a multiphase jet machining (MJM) technology was proposed by Su et al. (2016), in which a mixture of abrasives and water was accelerated by compressed air through a miniature nozzle to remove material from substrates. Shi et al. (2017) pointed out that MJM technology can not only take advantage of AAJ under relatively low pressure but also solve the problems of environmental pollution. By dissolving abrasives in water, the consumption of abrasives is reduced, and valuable abrasives can be recycled. Subsequently, feasibility in surface texturing was well verified by Hu et al. (2020a, b). However, there are some unknown issues with MJM as a potential manufacturing technique. What are the effects of the water added? In addition, according to the literature search, some techniques are similar to this method, and their technological differences must be compared comprehensively.

In this paper, the unknown characteristics of MJM were experimentally investigated by a comparison with the absence of water (equivalent to one of dry AAJs). Parameters compared between these methods include jet characteristics (structure, diameter, machining

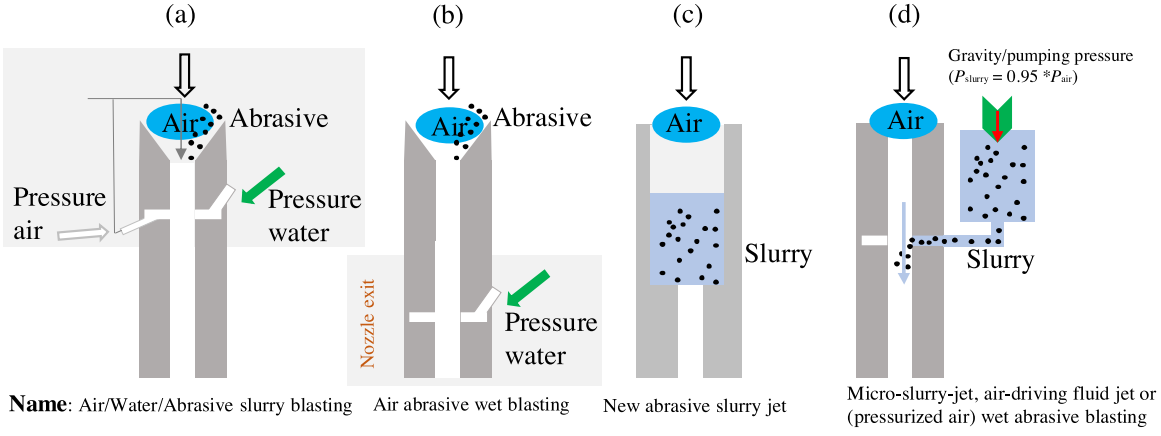

Fig. 1. An overview of various types of wet AAJ nozzle.

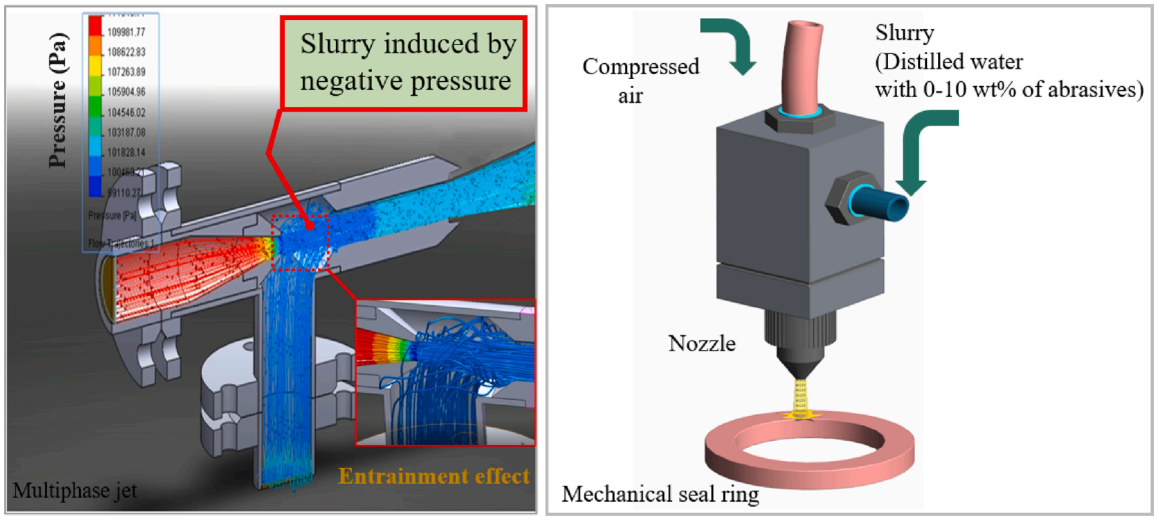

Fig. 2. Schematic diagram of the formation of MJM.

footprint, etc.) and some important features of the generated dimples or surfaces.

2. Analysis and comparison

2.1. Technique difference of MJM

As shown in Fig. 1, there are also similar machining methods that mix water and abrasives with air. They are referred to here as wet abrasive air jets (wet AAJs), although different researchers have given them different names. The variations in ways of mixing the three phases determine the characteristics and application of the jet. Table 2 summarizes the results reported in the literature for all kinds of nozzle designs and their applications.

The early forms of wet AAJ are shown in Fig. 1(a–b) (Old and Heitbrink, 2007), in which pressured water is introduced at the nozzle upstream or exit. Fig. 1(c) shows a special slurry jet machining system proposed by Nouraei et al. (2013), in which the slurry is pushed into a small tube by compressed air, making it more like an ASJ; thus, the slurry jet machining system yields a "W"-shaped erosion profile under certain operating parameters. Fig. 1(d) shows the most frequently used wet AAJ, in which air passing through a relatively large and straight tube (3–8 mm diameter) results in a weak entrainment effect; thus, sometimes the transport of the medium is conveyed with an additional pumping pressure (Iwai et al., 2009). This type of wet AAJ technique is similar to pumping air into the ASJ to form bubble flow with a cavitation effect and was first used by Iwai et al. (2009) to test the wear resistance of coatings. Then, Tsai et al. (2008) modified the technique by using a 4-mm nozzle size to form a large mixed jet flow. Due to its characteristics of low speed and large cover zone, the slurry jet machining system was used to polish the electrical discharge (ED) machined surface, including Tsai et al. (2008, 2009, 2013) and Yan et al. (2008). Most recently, the slurry jet machining system was also used for abrasive jet polishing of free-form machined surfaces such as the inner surfaces of microgrooves and linear/curved microchannels (Mao et al., 2010). Additionally, SiC or wax-coated SiC particles within pure water (Tsai et al., 2009), water-solvent machining oil (Tsai et al., 2008), water wax (Mao et al., 2010), or their mixture (Yan et al., 2008) were added to the air supply to improve the ED-machined surface. Other related applications using the method shown in Fig. 1(d) include Bouzakis's work, in which cutting edges were prepared (Bouzakis et al., 2011); Nakanishi's work, in which the wear behavior of wet AAJ machined surfaces was tested (Nakanishi et al., 2015, 2017, 2018); and Baba's work, in which fracture-free surfaces on the target materials of lithium metasilicate glass-ceramic and dental ceramics were obtained (Baba et al., 2019).

The proposed multiphase jet machining (MJM) technology is shown in Fig. 2. Structurally, the MJM used a combined nozzle consisting of a convergent air nozzle, a mixing chamber and a conical focus tube. The ratio of ambient pressure to internal pressure at the convergent air nozzle (diameter of 0.7 mm) results in an increase in air velocity and a strong negative pressure in the mixing chamber, which can be described by the Bernoulli equation of compressible flow. The premixed slurry (abrasive and water) can be drawn into the mixing chamber by negative pressure and then mixed with the air jet to accelerate the formation of a multiphase jet that flows through the focus tube with an inner diameter of 1.9 mm. The increased velocity and the small focus tube can facilitate the micromachining capacity of the surface texture. The strong negative pressure allows easy suction of the slurry without the need for additional pumping pressure. Based on the active suction process, the net result is a more thorough mixing of gas-liquid-solid than other methods presented in Fig. 1(a–d) and changes the jet structure, which will be described in detail in Section 3.1.

2.2. Unknown issues of MJM

As mentioned above, previous studies of wet AAJs have focused mainly on surface polishing, and only little attention has been given to the micromachining of surface textures, where the feature details are of greater concern. In fact, water in MJM technology may play an important role, and there are many unknown issues:

1) Haghbin et al. (2015) and Messelink et al. (2005) found that the introduction of air into the abrasive water/slurry jet would significantly increase the material removal rate but enlarge the jet diameter and make the polished surface have deeper surface defects. Then, is it possible to reduce the air jet diameter and improve the surface finish by introducing water into the air jet? How does introduction of water affect other surface characteristics such as machining profile and surface hardness?
2) No comparisons to the dry condition were made for the surface texturing. The effects of water on the surface roughness were not sufficiently illustrated. To what extent is reducing the surface roughness accomplished within the texture made by wet conditions versus dry conditions? This question is addressed in the context of micromachining of surface texture, which is central to this study.

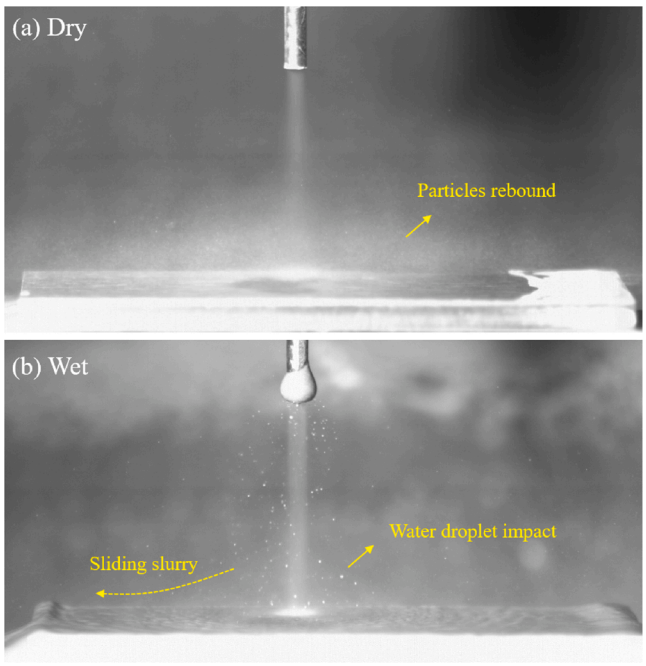

Fig. 3. High-speed camera images of (a) dry and (b) wet conditions using 0.6-MPa jet pressure and 13-μm particle size.

3. Experimental results and discussion

3.1. Jet structure

To investigate the unknown effects on jet structure, machining footprint, machining profile, and surface roughness when water was used (wet condition) or not (dry condition), a series of comparative experiments was conducted using specially designed multiphase jet machining equipment as reported in our previous work (Hu et al., 2020a). By using a valve under the same conditions, the inflow rate of dry abrasive particles (without using any liquid additive) was regulated to be the same as the premixed slurry (abrasives uniformly distributed in water, ~10 wt % abrasives).

After the secondary flow (dry abrasive or premixed slurry) was inhaled and accelerated by the high-speed airstream, the mixed flow passed through the focus tube to form the jet flow. Fig. 3 shows images of jet flow captured by a high-speed camera (i-SPEED 716, iX Inc., Tokyo, Japan) under dry and wet conditions. Under dry conditions, as shown in Fig. 3(a), the boundary of the jet is vague, particularly in the area near the substrate, where the accelerated dry abrasive particles rebound immediately after hitting the target surface. Around the jet impact zone, a large number of rebounding particles are suspended in the air, which will cause pollution and difficulty in abrasive recycling. Under wet conditions, Fig. 3(b) shows that the jet boundary is relatively clear, and the jet seems to be more convergent than under dry conditions. Many droplets with different sizes are found in the high-speed airflow. The environment around the jet is clean and has no violent particle rebound phenomenon. Away from the impact zone, both sides can observe sliding slurry and advancing ripples on the target surface.

Why were droplets formed under the wet conditions? Huang et al. (2012) found that during an ultrahigh-pressure waterjet (WJ), breakdown of the jet into some droplets starts to occur once the water jet departs from the nozzle exit due to aerodynamic interactions, turbulence and cavitation. Leu et al. (1998) described that the initially coherent jet can break up fully to form droplets as air is entrained into the AWJ. Compared with the waterflow, the same but more intensive entrainment effect can also occur in the compressible airflow. Thus, due to the strong cavitation within the mixing chamber of the MJM, the fluid will be completely exhausted to form droplets after the slurry enters the nozzle under negative pressure. Since the water droplets have a certain viscosity and adsorption capacity, the small particles will be wrapped in them and accelerated together with the airflow to eventually hit the workpiece. Obviously, the wet condition is characterized by a large number of droplets containing particles in a high-speed air flow, which is a typical three-phase flow, while the dry condition is a two-phase flow.

It also needs to illustrate the difference between the air-based MJM and water-dominated jet techniques shown in Table 1, because there are three similar phases containing gas, liquid and solid in these jets. These three-phase flows include mainly the air entering the abrasive water jet, the ultrasonic or self-oscillating abrasive water or slurry jets (PWJ), and the entrainment of surrounding air after the water jet exits the nozzle. However, in these water-dominated flows, either the gas composition is low or the flows are filled mostly with bubbles rather than droplets. When compared with other wet AAJs shown in Fig. 1(a–d), only the method shown in Fig. 2 causes a strong negative pressure that can atomize the liquid into water droplets, while a positive pressure or weak negative pressure obviously cannot. The addition of water to the MJM changes the formation and composition of the jet, and the resulting effects will be investigated and discussed.

3.2. Machining footprint

Fig. 4(a) presents optical images of the machining footprint using dry and wet conditions on the silicon (Si) substrate. The nozzle was fixed at a certain height of 1–13 mm from the workpiece. The machining conditions were air pressure of 0.6 MPa, jet angle of 90°, particle size of 13 μm, and processing time of 1-minute. Due to the divergence of the jet and the secondary impact after the particle rebound, there is a bright area around the edge of the machined dimple, the so-called frosted zone. Fig. 4(b) shows the frosted width and dimple diameter as a function of jet distance, which is drawn according to the machining footprint size of Fig. 4(a).

Under dry conditions, the rebound of particles is too violent. Most particles will fall to a distance after being bounced into the air, so there are almost no erosion marks caused by the secondary impact of particles around the dimple. The frosted zone under dry conditions is caused mainly by divergent flow. As the jet distance increases, the divergence becomes severe, resulting in a more blurred dimple edge and a larger width of the frosted zone.

Interestingly, under wet conditions, the addition of water makes the edge of the dimple clear, and the width of the frosted zone is significantly reduced. Taking the jet distance of 13 mm as an example, with water used, the frosted zone can be reduced from 9.54 mm to 5.04 mm. As shown in Fig. 4(b), the frosting under wet conditions first decreases and then increases, achieving a small frost zone at the 4-mm jet distance. The large frosted width at the jet distance of 1 mm is due to erosion caused by the secondary impact of particles around the dimple. Therefore, in addition to a bright area around the dimple, there is also a shallow erosion area (see Fig. 4(a)). The bright area is caused by the divergent jet, while the shallow erosion area is caused by the secondary impact of particles. As the jet distance increases, the secondary impact ability of the particles decreases, resulting in a decrease in the shallow erosion marks, and these marks are increasingly covered by the erosion caused by the divergent jet.

Fig. 4(b) also shows that when the jet distance is less than 10 mm, the dimple diameter under the wet condition is slightly smaller than the dimple diameter under the dry condition. When the jet distance exceeds 10 mm, the machined diameter under the wet condition is close to the machined diameter under the dry condition and even exceeds the machined diameter when the jet distance is 13 mm. Without considering the particle rebound, the jet structures under dry and wet conditions are drawn in Fig. 4(c) based on the experimental results, clearly showing the convergent effect of the jet flow when using water. These machining results reveal that the addition of water can slightly decrease the

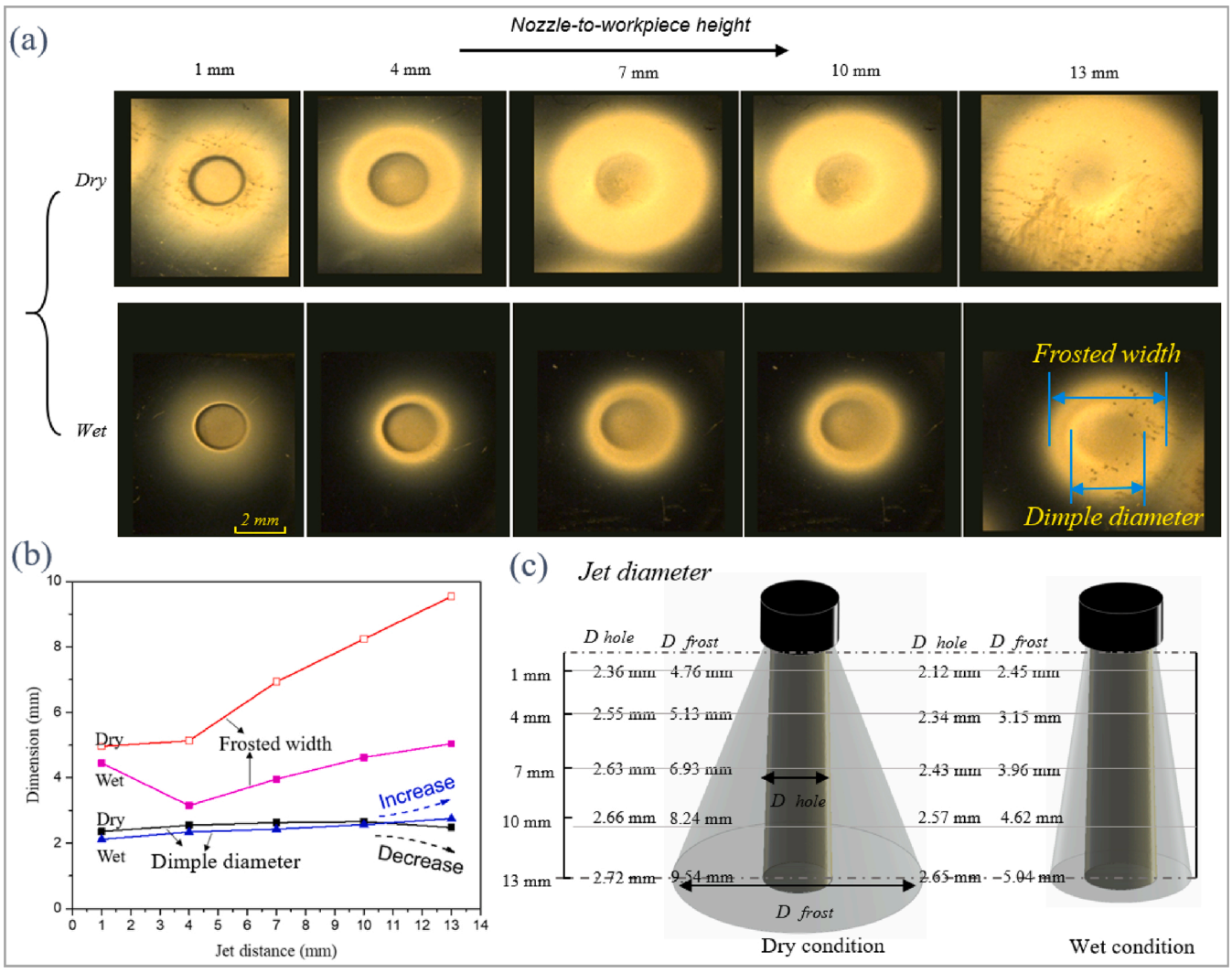

Fig. 4. Comparisons of (a) machining footprint measured by a digital microscope (KEYENCE Inc., Osaka, Japan), (b) frosted width and dimple diameter and (c) jet diameter between the dry and wet conditions.

diameter of machined dimples and obviously decrease the frosted zone, thus improving the boundary resolution.

Humphrey et al. (1990) reported that the momentum equilibration number, λ, can be used to assess the extent to which entrained particles follow fluid flow streamlines, expressed as:

$$\lambda = \frac{\rho_p (d_p)^2 v_{jet}}{18\mu(d_f)} \quad (1)$$

where ρ_p is the particle density, d_p is the particle diameter, v_{jet} is the jet velocity, μ is the dynamic viscosity of the fluid, and d_f is the focus tube

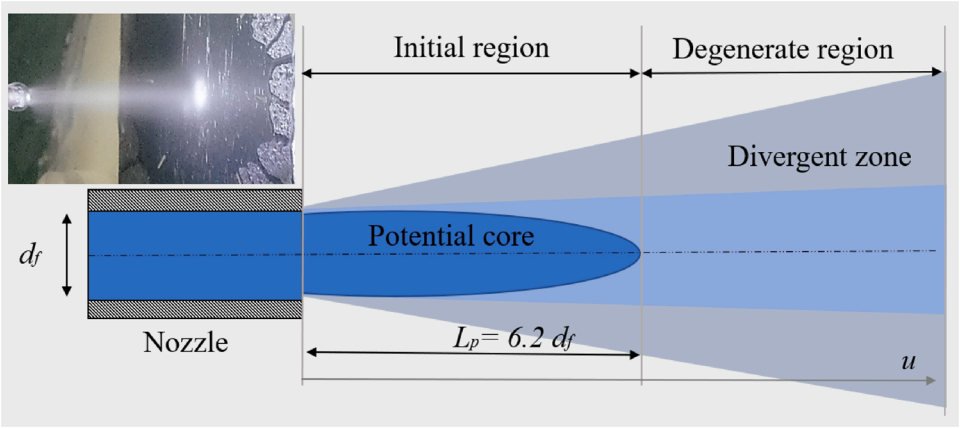

Fig. 5. Structure of the free air jet flowing in the air (not to scale) (Li et al., 2009).

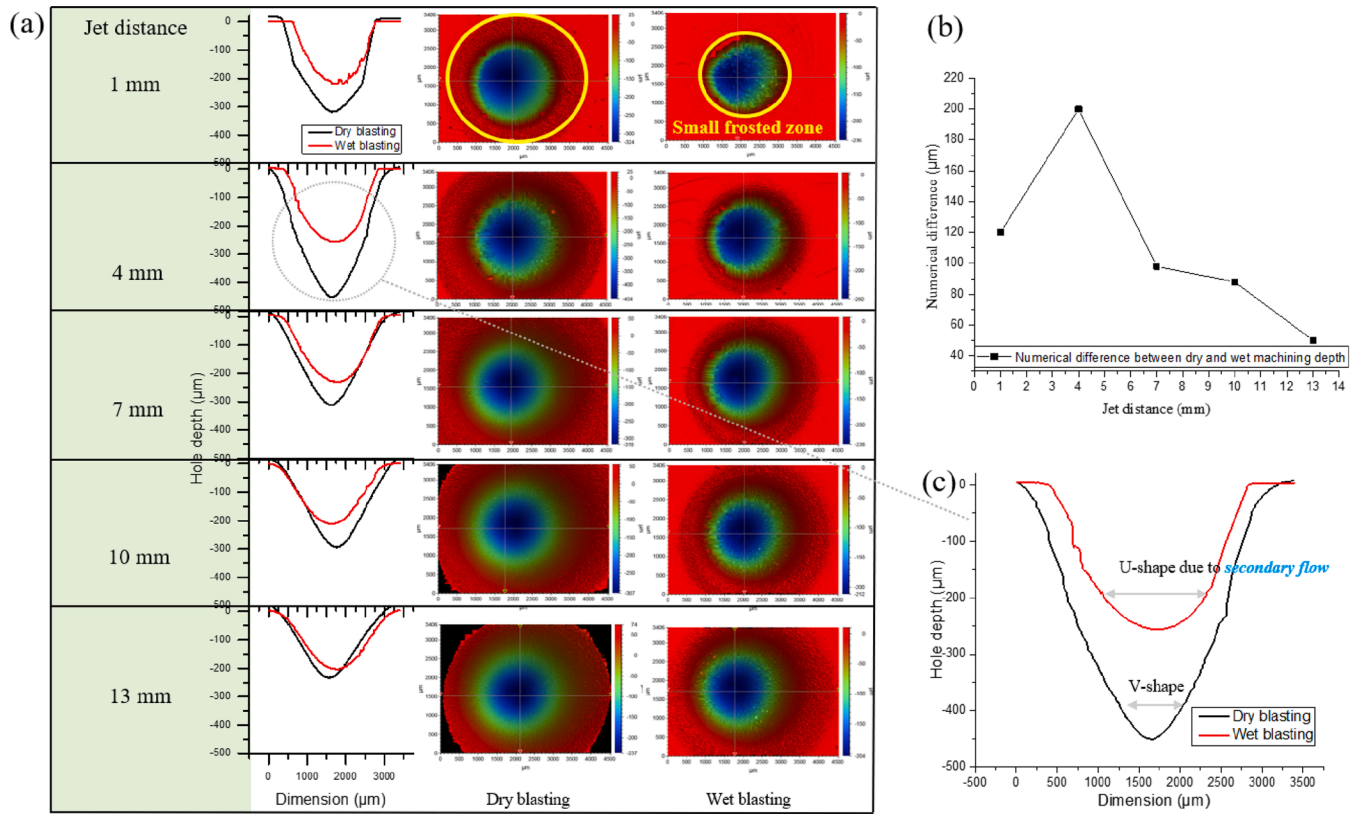

Fig. 6. (a) Machining profiles of dry and wet condition, (b) graph of numerical difference between the depth of dry and wet condition with the variation of jet distance, and (c) an enlarged comparison diagram at jet distance of 4 mm in (a).

diameter. During wet conditions, many of the small particles are wrapped in the droplets, which is equivalent to increasing the equivalent diameter of the particle. The increase in λ indicates that the large droplets tend to follow their original trajectory without being deflected by the divergent flow field in the covered area. That is, the addition of water causes the air jet to converge and limits the deflection of the particles; thus, it is beneficial for micromachining. The aerodynamic focusing method presented by Luo et al. (2019) is also beneficial to reduce the dimple diameter machined by abrasive air jets, but that aerodynamic focusing method increases the frosted width. Comparatively, the significant advantage of the MJM method is that it not only reduces the machined dimple diameter but also greatly reduces the frosted zone width.

Fig. 5 shows the structure of the free air jet flow in the air. As is known from ref. (Li et al., 2009), the axial distance u from 0 to 6.2 d_f is usually described as a potential core, where the air flow velocity is considered to be constant. When the jet distance reaches the end of the potential core (6.2 d_f= 11.78 mm), the air jet starts to enter the degenerate zone. Thus, under dry conditions, when the jet distance reaches 13 mm, the boundary of the machined dimple becomes very blurred. Under wet conditions, the water flow breaks up fully to form droplets and accelerates together with the airflow. Fine particles are wrapped in the water droplets. In macroscopic observations, the particles can be regarded as flowing in an environment of water. Of course, the viscosity of this mist fluid is much lower than the viscosity of pure water. In general, many researchers have pointed out that water or slurry jets have a smaller jet divergence and longer potential core length (*approximately 100 d_f*) than air jets because the viscosity of water is approximately 100 times the viscosity of air. Obviously, water was introduced into the air jet to make it similar to the slurry jet. Compared with the dry conditions, due to the increase in viscosity and restriction of water droplets during the wet condition, fine particles will easily move along the jet centerline with a small divergence angle and form a long potential core length (*Lp*). In other words, the attenuation of the dry air jet is more significant than the attenuation of the wet air jet as the jet distance increases. Thus, under wet conditions, when the jet distance reaches 13 mm, the boundary of the machined dimple is still clear, and the machined dimple diameter tends to increase. With the water used, the air jet will be changed to have a small divergence zone and a fine but long potential core.

3.3. Machining profile

The last section shows that additional water can affect the trajectory of particles associated with machining. Then, how does it affect the machining profile? Under the conditions of air pressure of 0.6 MPa, jet angle of 90°, particle size of 13 μm, and processing time of 1-minute, the erosion profiles machined under dry and wet conditions at different jet distances are compared in Fig. 6. The machining profiles and surfaces of disintegrated dimple were evaluated using a 3D optical profilometer (BRUKER Inc., USA).

As shown in Fig. 6(a), under both dry and wet conditions, when the jet distance increases, the erosion depth first increases and then decreases, achieving a maximum erosion depth at an approximately 4-mm jet distance. The erosion depth under wet conditions is smaller than the erosion depth under dry conditions. A small-frosted zone width can also be observed clearly from the 3D surface under wet conditions. Fig. 6(b) presents the numerical difference between the machining depths under the dry and wet conditions. With increasing jet distance, the difference first increases and then falls. Fig. 6(c) shows an enlarged comparison diagram when the jet distance is 4 mm in Fig. 6(a), comparing the normalized profiles of holes machined using dry and wet conditions. The cross-sections of holes in Si wafers machined under dry conditions are typically “V” shaped, while there is a more “U”-shaped cross-section under wet conditions, with sidewalls that are steeper than the sidewalls under dry conditions. These machining differences will be

Table 3
Parameters for simulation modeling of jet machining.

Fluid inlet velocity	100 m/s (Iwai et al., 2009)
Particle inlet velocity	100 m/s
Outlet pressure	0 Pa
Reference pressure	101,325 Pa
Particle shape factor	0.76
Average density	1.225 kg/m^3
Dry viscosity	1.7894e-5 kg/m s
Wet viscosity	1.7894e-4 kg/m s

illustrated by the erosion mechanism in the next section.

3.4. Erosion mechanism

Material erosion is a complex process in which the solid particle impact is affected not only by the sphericity, size and impact velocity of the particles but also by the mass flow rate, particle distribution and local impact angle distribution incident on the substrate, which in turn depends on the movement trajectory of particles.

The change in the machining profile is related to the movement trajectory of particles near the target surface. Obviously, the increased viscosity under wet conditions can make the particle motion behavior more complex. To qualitatively understand the particle motion details in the dry and wet jet impact zones, a series of simulations were performed in this study using ANSYS Fluent 16.1 (ANSYS Inc., Cecil Township, PA, USA). Several assumptions were made in this simulation: the air stream is steady flow; the added water was thought to increase the density and viscosity of flow; the particle concentration is relatively small, so its influence on air flow can be ignored, and the collapse between particles can be excluded. Because the low concentration of particles significantly eliminates particle-particle and particle-flow interactions, particles are injected through the medium at the same velocity as the fluid, following the k-ε turbulence model. A unidirectional coupled Lagrangian discrete phase model (DPM) was used to simulate the flow field of viscous fluid and trace the particle trajectories in the stagnation zone. A second-order upstream discrete scheme was used for numerical stability. Hexahedral cells were used to mesh the fluid domain with cells arranged roughly in the direction of the jet to reduce false diffusion between cells. The mesh was refined near the target surface to capture the particle motions. The viscosity of the dry conditions is equal to the air viscosity. It is difficult to obtain the viscosity under wet conditions; hence, the average viscosity was assumed to increase tenfold. The walls of the target and focus tubes were treated as smooth no-slip walls. The jet velocity was regulated by the air pressure, from 0 to 0.6 MPa. According to Iwai's research, the nozzle exit velocities at 0.6 MPa were estimated to be slightly over 100 m/s (Iwai et al., 2009). The model was initially assumed to be filled with air, and no slip existed among the phases in this model. Table 3 gives the boundary conditions of the solver used in the simulation.

The simulation was carried out while the dimple initially formed. Fig. 7 shows the absolute pressure, velocity and particle trajectory contours of dry and wet jet flows within the formed dimple. Fig. 7(a) compares the absolute pressure clouds of the two jets. A high-pressure zone is formed at the bottom of the dimple, the so-called stagnation zone. The stagnation zone under wet conditions is stronger than the stagnation zone under dry conditions. At the same time, a low-pressure area is formed at the boundary of the dimple (see details A and B). The boundary pressure under wet conditions is lower than the boundary pressure under dry conditions, which can affect the formation of chamfers. In most cases, the chamfer under the wet conditions is smaller than the chamfer under the dry conditions.

Fig. 7(b) compares the velocity and motion trajectory of 13-μm particles under dry and wet conditions, revealing that the increased viscosity causes a large stagnation zone at the dimple bottom, which can

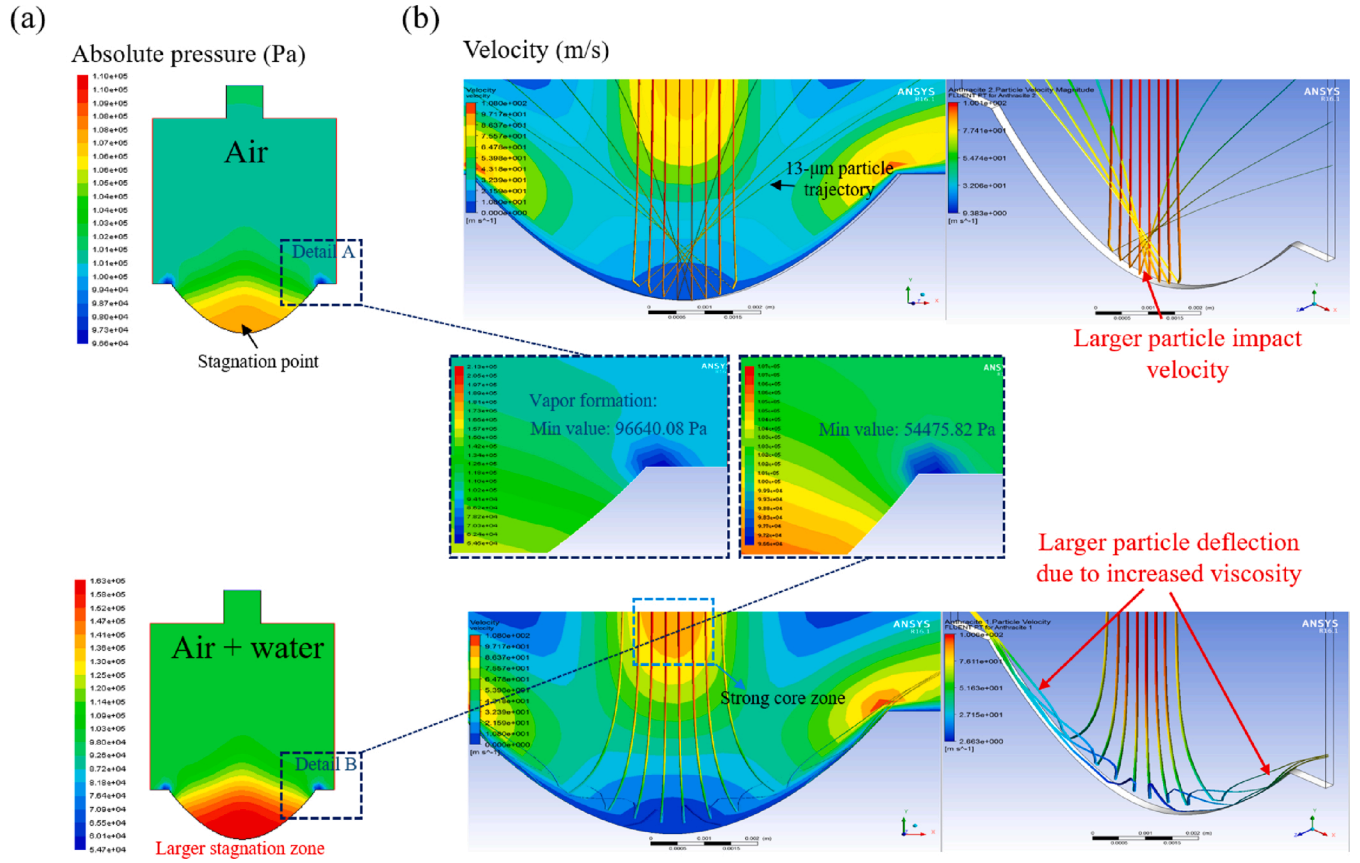

Fig. 7. Comparison of the (a) stagnation pressure and (b) particle motion near the impact zone between the dry and wet conditions.

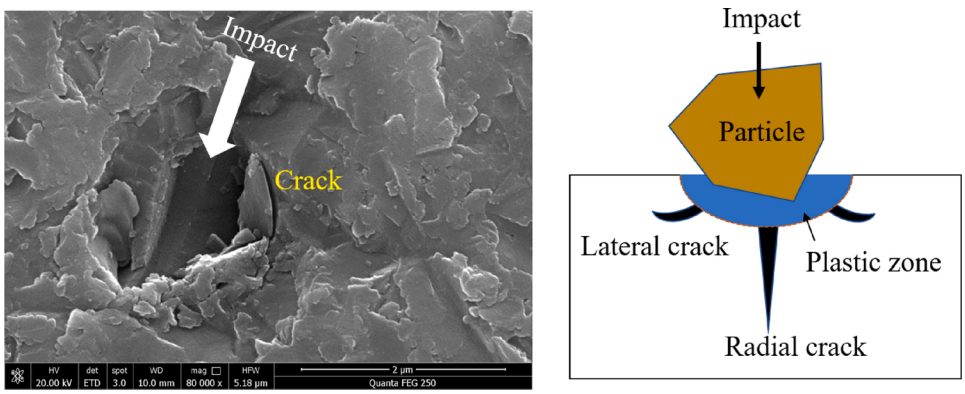

Fig. 8. The brittle erosion mode observed in the wet erosion of Si wafers using a field-emission scanning electron microscope (SIGMA 500, Zeiss) (Shi et al., 2017).

vary the particle impact velocities and angles. The strong stagnation zone can apply significant drag on the abrasive particles, reducing their impact velocities and thus, decreasing the erosion rate. Obviously, under the dry condition with a small stagnation effect, the interference with particles is small. A significant fraction of particles rebound immediately after hitting the target surface. This kind of rebound particle will seriously interfere with subsequent abrasive particles. Due to the strong stagnation effect upon jet impingement, the fluid diversion and velocity reduction under wet conditions are more notable than the fluid diversion and velocity reduction under dry conditions, and the particle rebound ability is significantly reduced. The particle impact velocities and angles at the jet center and jet edge are different. Most of the particle trajectories incident perpendicular to the surface will deflect radially, causing these particles to move away from the centerline and strike the surface at a shallower angle. The net result is that at the center of the jet, the flux of impacting particles is relatively low, and the local impact

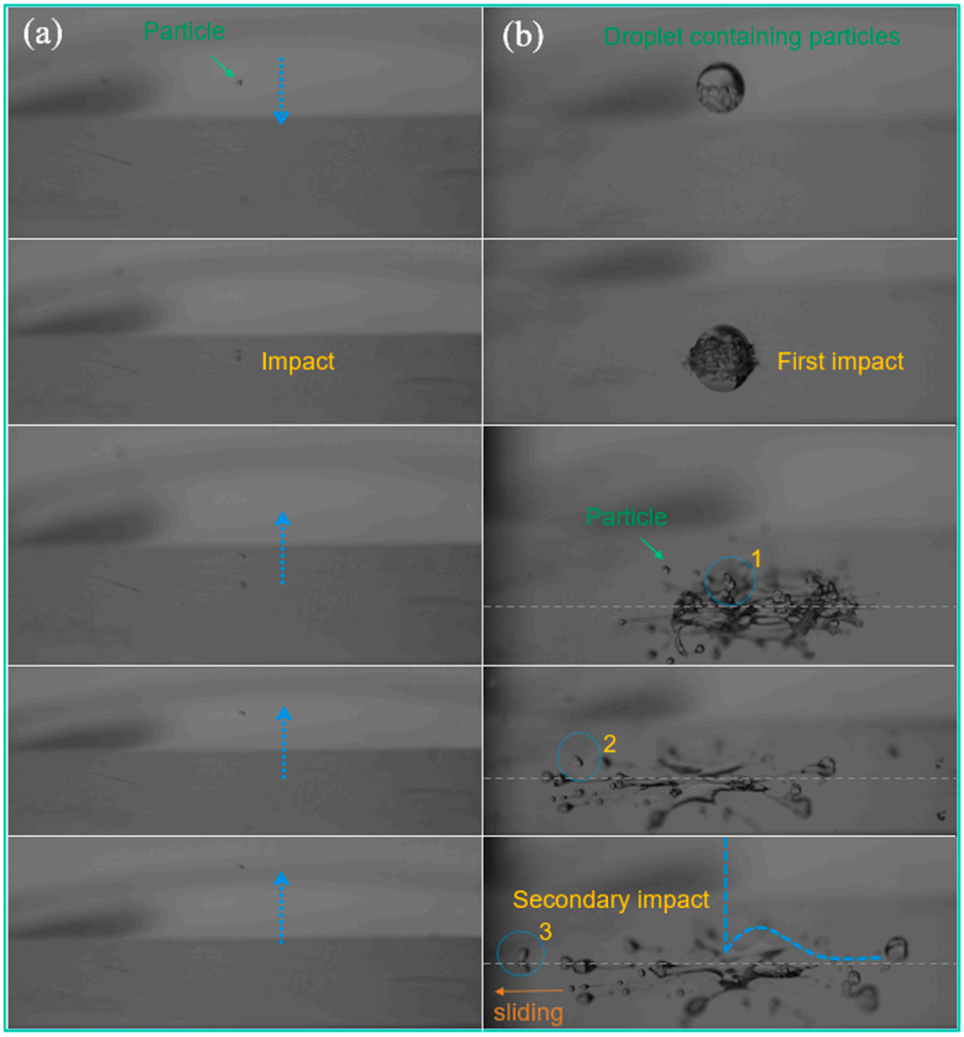

Fig. 9. Instantaneous motion pictures of particles impacting the surface of the workpiece captured by the high-speed camera (i-SPEED 716, iX Inc., Tokyo, Japan) under (a) dry and (b) wet conditions. (The blue dotted line represents the continuous movement of particles).

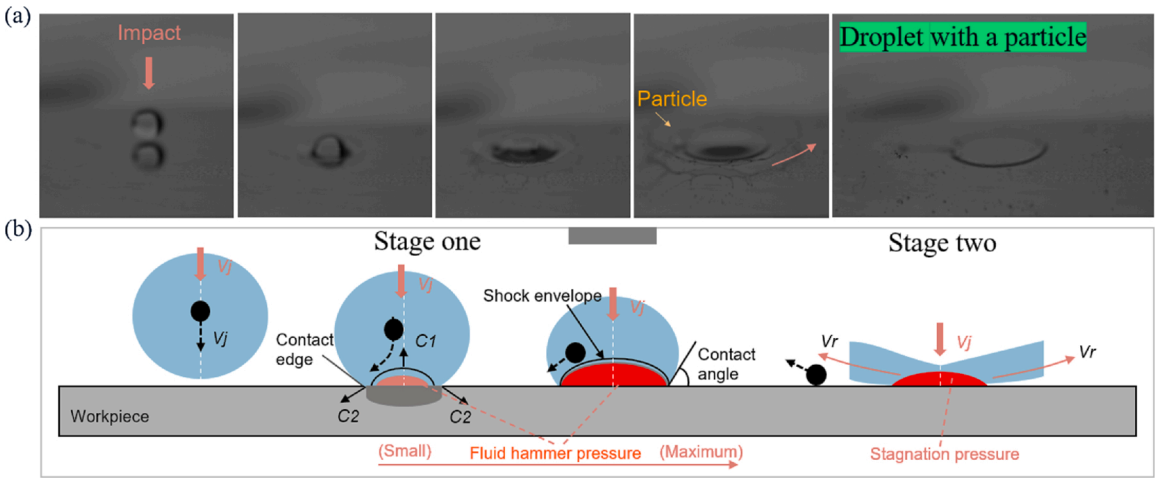

Fig. 10. (a) Photos and (b) schematic illustration of the high-velocity impact of a water droplet containing a particle on a solid surface.

angle varies across the jet. Specifically, the impact angle is close to 90° (that is, vertical) in the center area, but the impact angle becomes increasingly shallow at the distance away from the jet centerline where the secondary flows move more parallel to the dimple surface. Obviously, the dimple wall formation is related to this particle deflection and secondary flow along the dimple surface. Compared with the dry jets, the wet jets will form "U"-shaped dimples with a wider bottom because some deflecting particles with a larger impact angle first hit the sidewall surface directly and more secondary particles flow along the sidewalls of the dimple.

Near the stagnation zone, due to the increased viscosity, the particle impact velocity under wet conditions shows a slight decrease (see Fig. 7 (b)). The erosion of Si wafers is a typical brittle erosion mode based on the solid particle erosion surface shown in Fig. 8. Since the erosion rate of the brittle mode is generally lower at these shallower impact angles, the local erosion rate of the wet conditions is lower near the jet center than the local erosion rate under dry conditions. In this way, the particle-indented depth may decrease, thus resulting in a shallow and "U"-shaped profile under wet conditions.

As mentioned earlier, the use of water makes the jet converge. This effect becomes particularly pronounced at relatively large standoff distances. Hence, at relatively large standoff distances, where the erosion is most affected by the wet jet with a small divergent angle, the two depths between the dry and wet conditions will be close to each other. At small standoff distances, the two depths are also close to each other, possibly because the subsequent abrasive can be seriously disturbed by the front bouncing abrasive under dry conditions. Both short-distance rebound and long-distance divergence will reduce the erosion rate under dry conditions.

In conclusion, under dry conditions, the vertical particle impact has a large removal efficiency, while under wet conditions, the deflected particles have the potential to improve the quality of the machined surface.

3.5. *Particle deflection*

The erosion mechanisms can be more accurately analyzed from a microscopic perspective. Fig. 9 shows instantaneous motion pictures of particles impacting the workpiece surface under dry and wet conditions. To clearly capture the particle movement details, relatively large glass beads for shot peening with a particle size of 200 μm and a low impact velocity were used. The flow speed may be different from the actual flow speed of 0.6 MPa, but complex near-wall particle flow can be well obtained to further explain the experimental phenomenon.

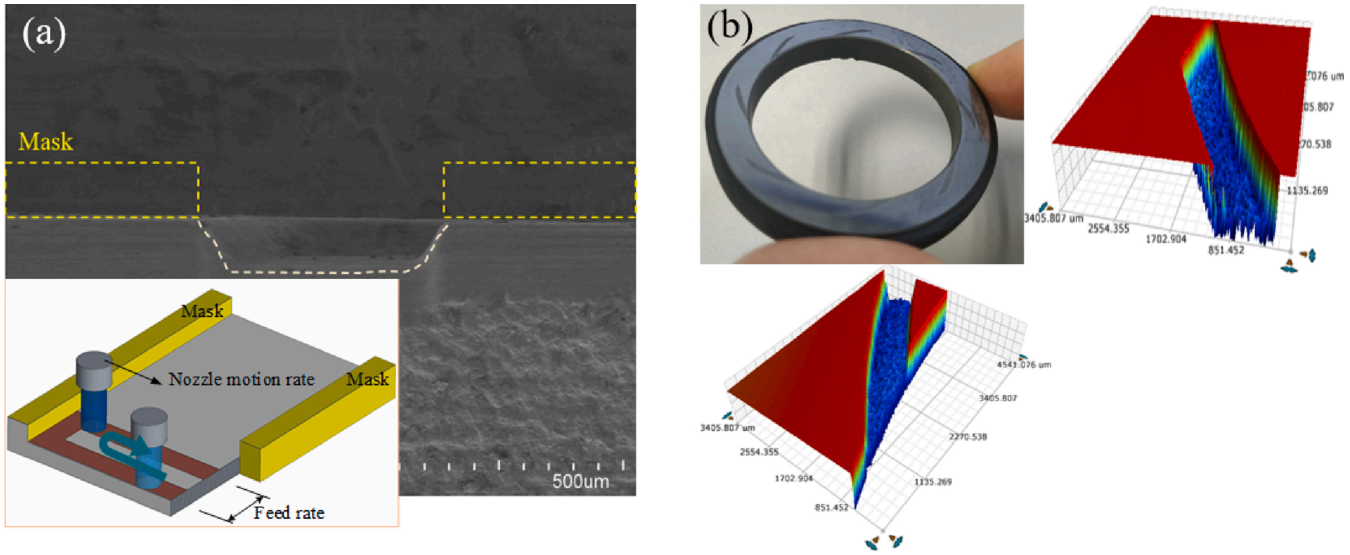

Fig. 11. (a) Scanning electron micrograph of a typical shallow channel machined using wet conditions with a S-type feeding path (Hu et al., 2020a), and (b) its 3D topography. (Experimental conditions: 90° jet angle, 13-μm SiC abrasive, 0.6-MPa jet pressure, 100-μm feed rate, 0.2-mm/s nozzle motion rate, 10-mm jet distance).

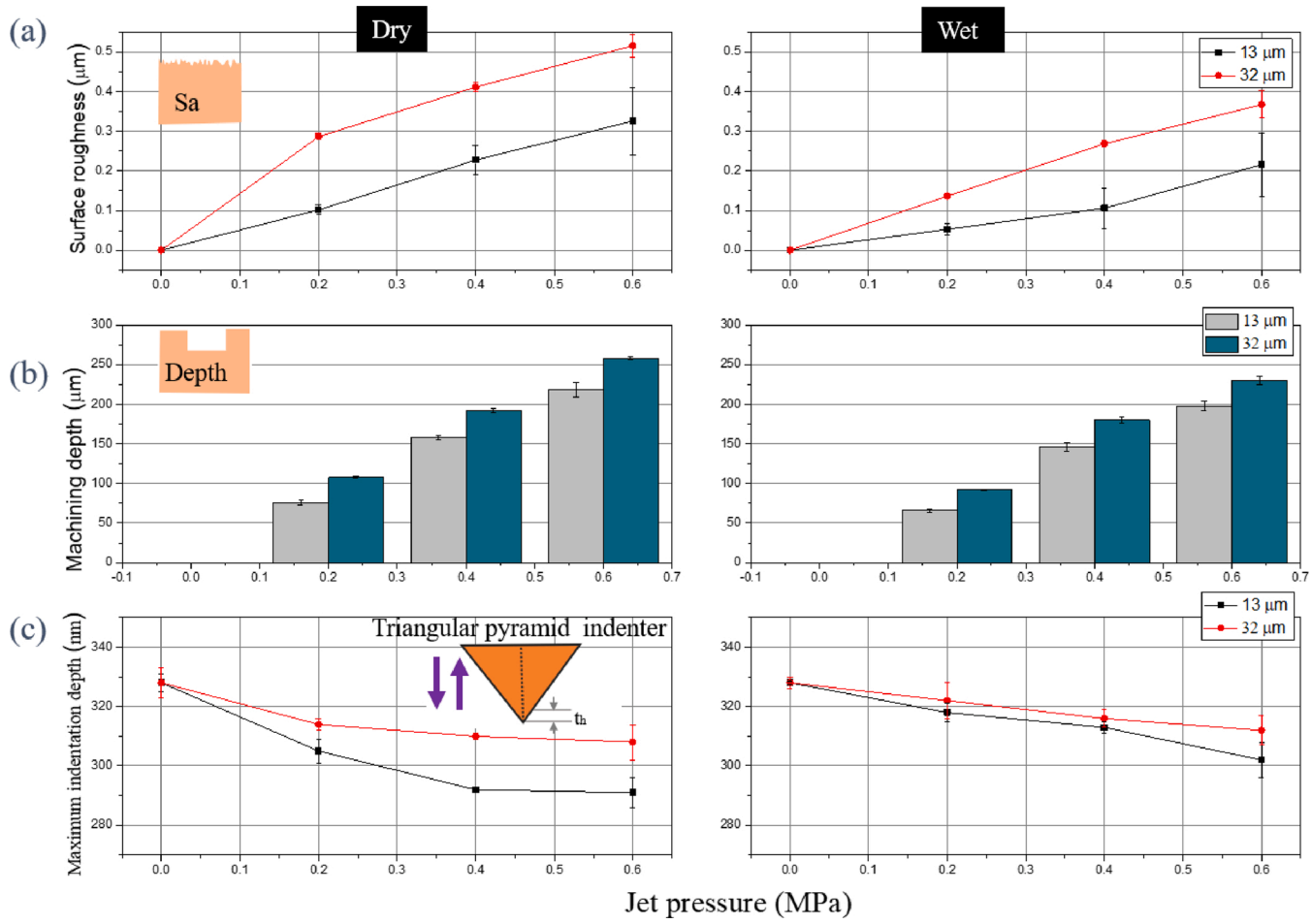

Fig. 12. Roughness, machining depth and nanoindentation results on Si wafers under dry or wet conditions via SiC particles of different sizes at various jet pressures.

Both particle trajectories of dry and wet conditions captured by the high-speed camera show good consistency with the simulation results shown in Fig. 7. As shown in Fig. 9(a), under dry conditions, the particles bounce from the surface almost perpendicularly after the first impact. The particle motions involved in the wet jet condition seem to be more complex, as indicated in Fig. 9(b). After the particle-containing droplets first hit the surface perpendicularly, most of the particles will go through three stages: (1) bouncing from the impact surface with a certain ejection angle; (2) flying in the air; and (3) hitting the workpiece again with a very low impact angle and then sliding on the machined surface. The movement of the particles across the surface produces an abrasive sliding scratch effect, which may improve the quality of the machined surface.

Why do particles deflect under the wet conditions? This complex near-wall particle deflection under wet conditions is related to the high-pressure zone formed by the droplet hitting the surface at a high speed. The impact contact between high-speed droplets containing a particle and a solid surface is illustrated in Fig. 10(a). The contact consists of two main stages, as shown in Fig. 10(b). During the first stage, because the shock velocity in the liquid (C_1) is lower than the shock velocity in the solid (C_2), at the moment when the droplet impacts the solid surface with a velocity of V_j, an area of high compressive pressure (short high-pressure transient, also called water-hammer pressure) will be generated due to the compression of the water. When the droplet is compressed until the shock waves reach the periphery of the droplet, the impact pressure reaches its maximum. Then, during the second stage, the shock wave eventually escapes from the contact edge, resulting in the release of the stress wave. At the same time, the water flows from the contact edge to both sides, and there is evidence that the outflow jet velocity (V_r) can be several times higher than the impact velocity (V_j) (Kong et al., 2010). Then, the impact pressure reduces to the stagnation point value. As shown in Fig. 10(b), the deceleration and deflection of particles are caused by the high-pressure zone, which has a dust-controlling effect and has a great influence on the abrasive erosion behavior.

3.6. Machining depth, surface roughness and hardness

In last section, experimental results indicate that wet conditions have the potential to improve machined surface quality. This section aims to further confirm the assumption through experiments. As shown in Fig. 11, by using a mask, miniaturized features with complex surface shapes can be fabricated. In addition, by using the S-type feeding mode, the machined features will obtain a flat bottom, which is convenient to measure the roughness and the average erosion depth. The S-type feeding mode was realized by moving the workpiece along the groove direction and synchronously oscillating the workpiece relative to the nozzle in the direction perpendicular to the mask edge. A metal mask with a thickness of 200 μm and an opening width of 500 μm was used. Other definite parameters were 100 μm feed rate, 0.2 mm/s nozzle motion rate, 90° jet angle, and 10 mm jet distance. The variable conditions were 13 or 32 μm SiC, 0.1–0.6 MPa jet pressure. The machining results are shown in Fig. 12.

As shown in Fig. 12(a–b), both under dry and wet conditions, SiC particles with an average diameter of approximately 13 μm seem to present lower roughness and smaller machining depth compared to the 32-μm average diameter. Fig. 12(a) shows that the machining depth of wet conditions is lower than the machining depth of dry conditions in

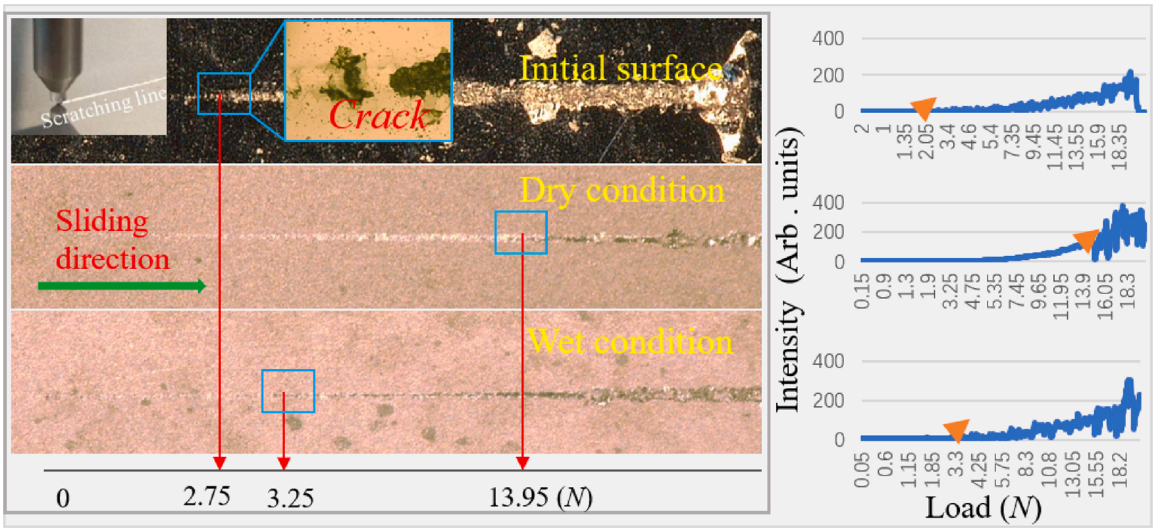

Fig. 13. Images of scratch tracks on the initial Si surface and the erosion surfaces under dry and wet conditions using a jet pressure of 0.6 MPa and particle size of 13 μm.

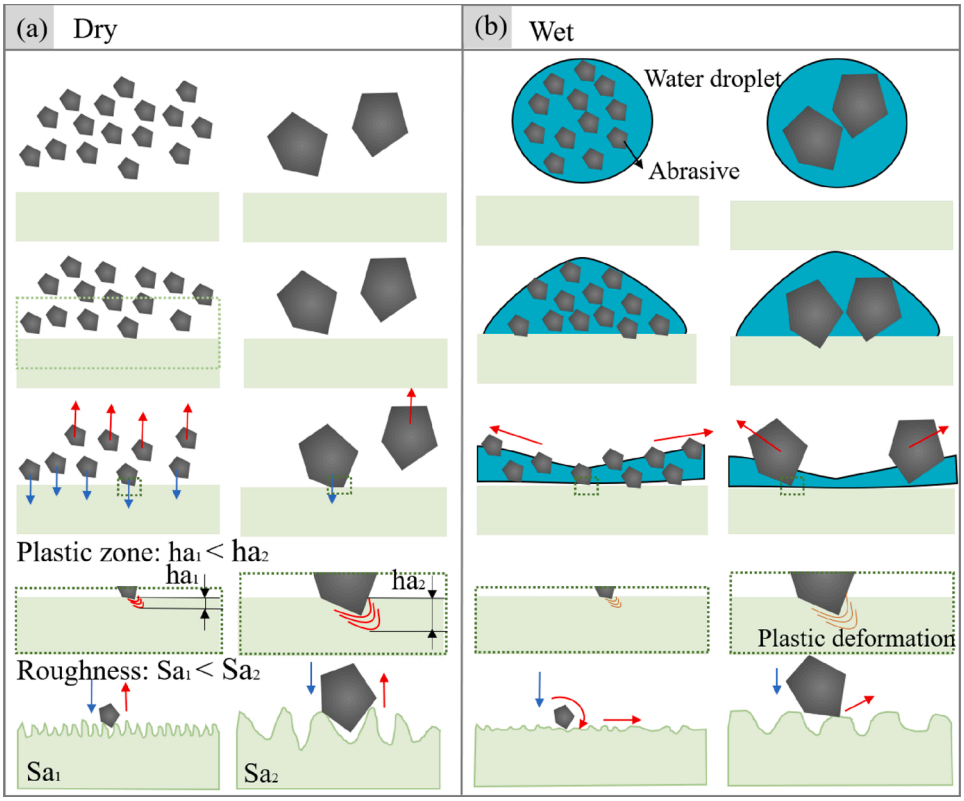

Fig. 14. The influence of abrasive particle size and its transport medium on the surface roughness under (a) dry and (b) wet conditions.

this erosion mode. Fig. 12(b) shows that the surface roughness under wet conditions is lower than the surface roughness under dry conditions, revealing that the added water does improve the quality of the machined surface.

For the surface texture, apart from the wear resistance caused by its geometric structure, the physical properties of the surface machined by abrasive jet machining also play an important role. Actually, the particle impact has a shot peening effect, which will cause a plastic zone below the impact point, as shown in Fig. 8. This effect will harden the surface, thereby improving the surface wear resistance. Therefore, it is necessary to explore whether the addition of water affects this characteristic.

The hardness of the eroded surface can be reflected by the nano-indentation depth, which was measured using a dynamic ultramicro hardness tester (DUH211 s, SHIMADZU, Japan) with a Berkovich indentation of 115°. Indentation with a constant test force of 20 mN was carried out on the substrate to test the maximum indentation depth. Fig. 12(c) shows that SiC particles with a small diameter seem to present a lower nanoindentation depth than SiC particles with a large diameter. The nanoindentation depth under wet conditions is also lower than the nanoindentation depth under dry conditions.

The wear resistance of the dry and wet jet machined surface was estimated using a scratch test with a loading speed of 20 N/m, loading

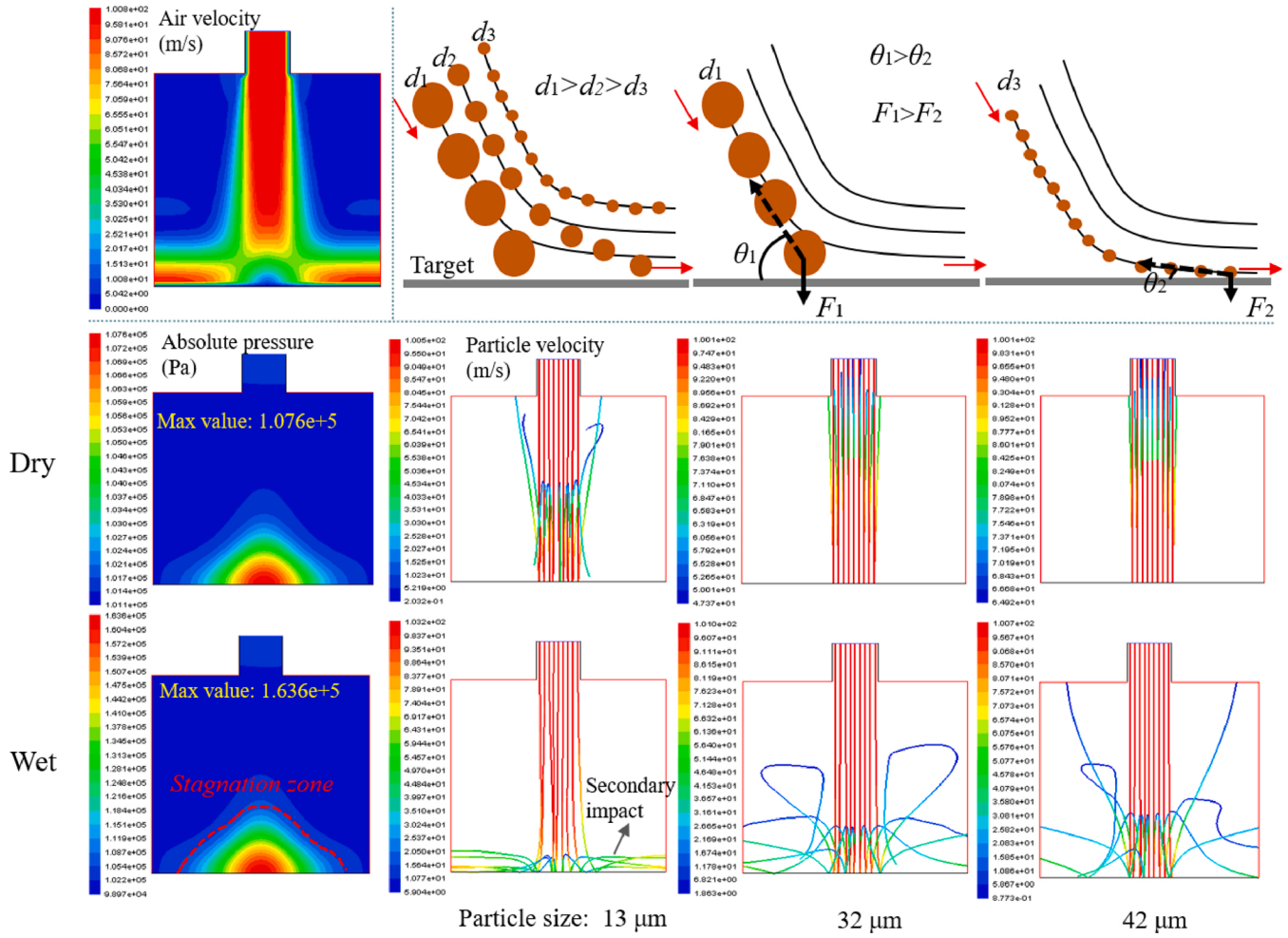

Fig. 15. The influence of abrasive particle size on the particle trajectories under dry and wet conditions.

force of 20 N and scratch length of 3 mm. The diamond loading head has a cone angle of 120° and radius of 0.2 mm. Fig. 13 shows that the wear resistance of the surface processed by both dry and wet conditions is improved, indicating that the hardened surface will prevent the emergence of scratch cracks. However, the addition of water will weaken this hardening effect, so premature fracture occurs on the wet machined surface. Scratch cracks and indentation depth are both a reflection of surface hardness, which means that the harder the surface is, the shallower the indentation depth and the shorter the plastic scratch length.

Fig. 14 schematically illustrates the effects of fine and coarse particles on the surface integrity of Si wafers under dry or wet conditions. Under dry conditions (see Fig. 14(a)), a larger roughness is generated if coarser particles are employed, illustrated by the repeated impacts on the Si surface by the coarser particles with relatively high erosion kinetic energy. Therefore, due to the more intense material removal ability through crack growth, the coarse particles cause severe plastic deformation and brittle fracture of the target compared with the corresponding fine particles. Beyond that, as theoretically shown in Fig. 15, fine particles are more likely to be deflected by the airflow and eventually impact the surface with a lower impact force and impact angle (F_2, θ_2) than coarse particles (F_1, θ_1). Since the brittle erosion of brittle materials depends strongly on the velocity component perpendicular to the surface and roughness decreases with the decrease in the normal impact velocity component and impact angle, the net effect of fine particles is to reduce erosion and therefore the channel depth, roughness and nanohardness.

The related mechanism of wet conditions is shown in Fig. 14(b). Under wet conditions, particles are easier to be deflected due to the high pressure formed in the impact of water droplets and eventually impact the surface with a lower impact force and impact angle than under dry conditions, so that the machining depth, roughness and nanoindentation depth under wet conditions are lower than under dry conditions. For wet conditions using fine and coarse particles, the machining difference can be well illustrated by the simulation results shown in Fig. 15. Under wet conditions, the direction of abrasive movement tends to be the direction of the water flow because of its large viscosity. For fine abrasive particles, this phenomenon of being guided by water droplets is more pronounced than using coarse particles. On the one hand, buffing occurs since small particles are dragged more easily by the flowing water along the surface, thus decreasing the first impact angle and improving the machining quality. On the other hand, a particle sliding effect occurring after the second impact also improves the quality. Large particles are less affected by water droplets and are used mainly to pierce materials deeper (see Fig. 15). A larger portion of the initial particle kinetic energy of the coarse particles is consumed to generate the deformation and crack system shown in Fig. 8. Thus, brittle material subjected to wet conditions by fine particles is considered to have a lower roughness and a smaller nanohardness than erosion by coarser particles under the same conditions.

3.7. Machining characteristics in sintered ceramics

In industrial applications, many materials are not the single-phase materials, such as Si. Most sintered materials have a nonuniform structure and are popular or potential materials of mechanical end seals owing to their high erosion resistance, high hardness and light weight.

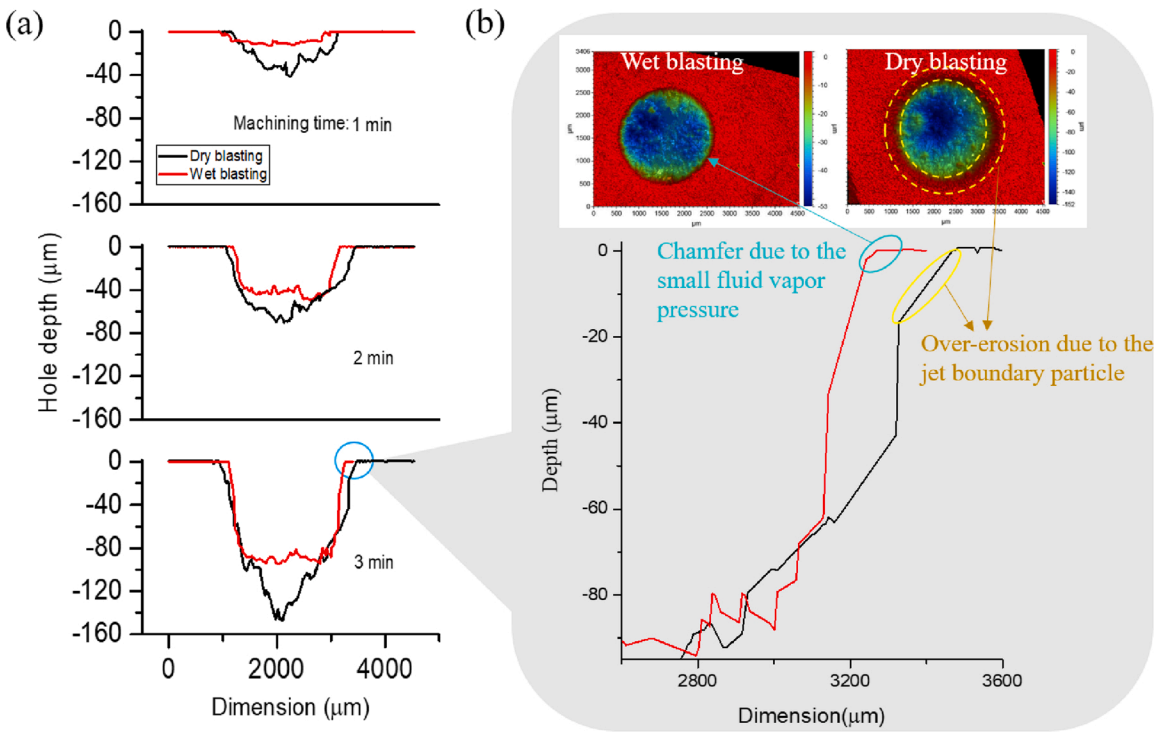

Fig. 16. Comparison of erosion profiles on cemented carbide (YG6) surfaces machined under dry and wet conditions using fixed jet mode, jet distance of 1 mm, jet angle of 90°, jet pressure of 0.6 MPa and particle size of 13 μm.

For example, cemented carbide is a compound ceramic, offering improved wear resistance as a result of a microstructure in which hard WC grains are surrounded by infiltration of the Co matrix. The heterogeneous mechanical and thermal properties caused by this uneven structure may affect the sensitivity of particle impact, so it is necessary to explore the erosion behavior of cemented carbide.

Fig. 16 shows that the addition of water has a more obvious influence on the machining profile of the cemented carbide. The results in Fig. 16 indicate that under the different processing times, the bottoms of the dimples processed under dry conditions are all relatively sharper, while the bottom surfaces processed under wet conditions are relatively flat. As explained in Section 3.4, this flat bottom under the wet condition is related to the large stagnation effect. This effect is more obvious in the machining of cemented carbide. It is found that the wet machined profile of the cemented carbide is flat, while the bottom of Si is rounded. In other words, under the wet condition, the machined profile of the cemented carbide is flatter than the bottom of the Si wafer, which may be related to the nonuniform force of the particles acting on the multiphase material. The same trend can be found in Kowsari's work, in which the glass and zirconium tin titanate were tested (Kowsari et al., 2016). In addition, the dimple machined under wet conditions has a smaller edge chamfer than the dimple machined under dry conditions, which can be obtained by the comparison between the blue and yellow areas of Fig. 16(b). The large chamfer during dry conditions may be caused by excessive erosion of the particles around the divergent jet boundary. Under the wet condition, a has low pressure and high velocity at the edge of the dimple (see detail B of Fig. 7(b)). Since abrasive particles were wrapped in water droplets and the slurry flowed rapidly at low boundary pressures, a small chamfer was formed under wet conditions.

Fig. 17 illustrates typical trajectories of the abrasive particles in dry and wet jet processes and presents SEM and 3D optical images of the corresponding machined surfaces. Compared with the machining results of the Si wafer in Fig. 12, the results of Fig. 17 show that when machining cemented carbide, the surface roughness of wet machining is obviously lower than the surface roughness of dry machining, revealing that the machining differences are magnified in the machining of sintered materials. The presence of hard and soft phases within the sintered materials leads to differing erosion behavior. Under dry machining, particles almost perpendicularly impact the target surface. Since the erosion rate of WC (brittle materials) is higher than the erosion rate of Co (ductile materials) at large impact angles, when particles hit the brittle phase vertically, the local penetration depth is too large, causing the pit depth to reach 4 μm. The protruding parts are Co materials that are difficult to remove, and the recessed parts are WC materials that are easy to remove. The average surface roughness of dry machining is 809 nm. Under wet machining, the breakage of droplets produces a lateral velocity several times greater than the impact velocity. Since the removal rate of Co (ductile materials) is higher than the removal rate of WC (brittle materials) at low impact angles, the protruding parts (Co) can easily be flattened by the particles with high lateral speeds.

In addition, in wet machining, abrasive particles are mixed with an additive (water solvent), which can easily cause the abrasive particles to slide over the surface following impact. Hence, as shown in Fig. 17(b), slight scratches can be observed on the wet erosion surface. The motion of the particles across the target surface generates a grinding polishing effect, and hence, the quality of the machined surface is improved. The sliding effect of liquid-coated particles is illustrated in Fig. 18, which results in the surface being flattened and smoothed. As shown in Fig. 17 (b), the height difference of the machined surface under wet conditions can be reduced to ±1 μm. The average surface roughness of wet machining is 312 nm.

These machining characteristics reveal that the presence of water can bring many benefits. Denkena and Biermann (2014) also reported that in slurry jets, water is considered to have a cushioning and damping effect that favors better surface quality, suppresses dust formation and has no thermally induced distortions. AAJ machining uses air as a carrier medium, which is a dry process. To improve the machining quality, researchers usually add a small amount of lubricating fluid such as minimum quantity lubrication (MQL)-assisted machining (Sen et al., 2019) in dry processing. Obviously, the added water in MJM was found to have the same lubrication effect.

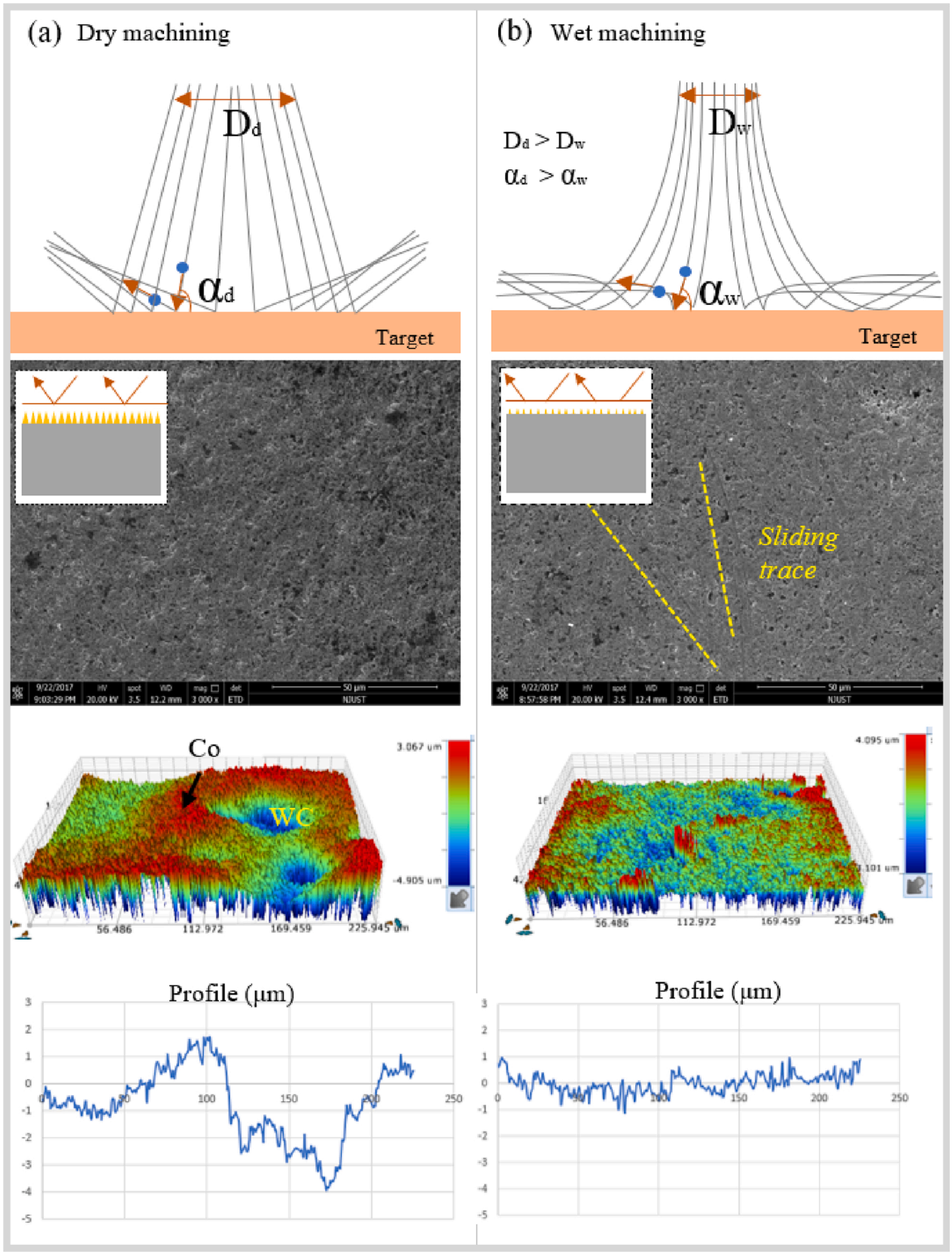

Fig. 17. The erosion surface on cemented carbide (YG6) under (a) dry and (b) wet conditions using the S-type feeding mode and the same conditions as in Fig. 16.

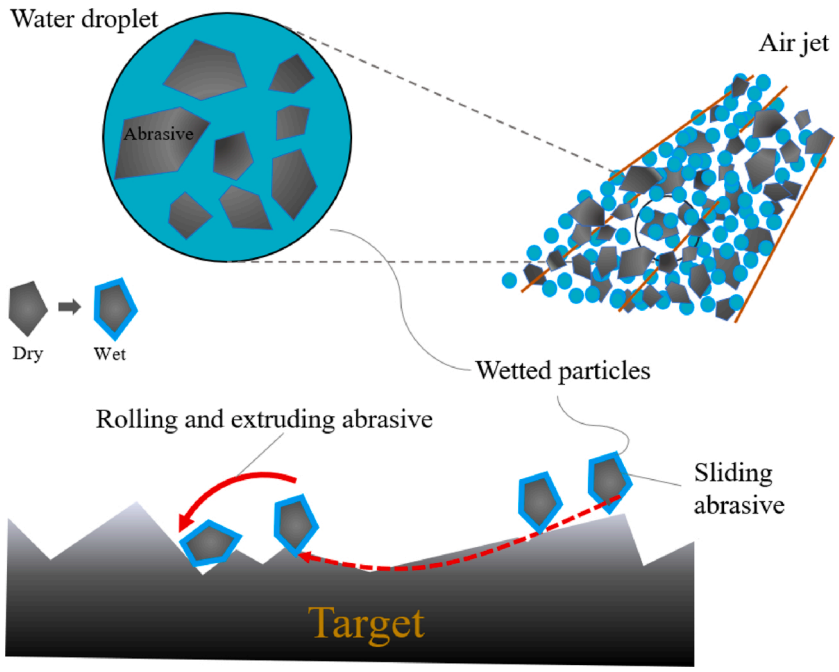

Fig. 18. Schematic diagram of the sliding grinding effect under wet conditions.

In summary, the novelty of this paper is that the proposed MJM method can be beneficial to ameliorate the technical microdefects such as dust dispersion, high surface roughness and large machining footprint size resulting from dry abrasive jet machining operations. According to the machining performance, MJM would be advantageous for the fabrication of tribological texturing on sintered ceramics, where both shallow features and a flat, repeatable depth are required. Despite several benefits seen in MJM, the use of this machine tool is limited due to the existence of some process limitations such as the entrainment method similar to abrasive water jets that results in lower energy transfer efficiency. Compared with abrasive air jet machining, experiments confirm that the addition of water in MJM further weakens the cutting force. Improvement of the machining efficiency during MJM will be the subject of past and continuing research.

4. Conclusions

Multiphase jet machining (MJM) is a recently developed surface texturing method that introduces water into dry abrasive air jet machining. To explore the effects of water added in MJM, we conducted a series of comparative experiments when water was used (wet condition) or not (dry condition). Dimples and masked channels were machined on Si and cemented carbide (YG6) surfaces to quantify the erosion rate, roughness and machining profile. Numerical simulations and high-speed capture images were used to help understand the particle erosion mechanism. The key concluding remarks in the comparisons of dry and wet conditions are as follows.

1 The added water was found to greatly change the jet structure. The MJM (wet condition) is characterized by a large number of droplets containing solid particle erodents within the high-speed airflow.
2 The MJM (wet condition) was found to have a very small divergent angle compared with the dry abrasive air jet. This convergent effect can reduce the jet diameter, thereby improving the machining resolution, manifested in the decrease in the machining footprint. Taking the jet distance of 13 mm as an example, with the water used, the machining footprint can be reduced by 47.2 %.
3 The added water obviously changes the particle motion trajectories near the target surface. Under dry conditions, particles almost perpendicularly bounce from the surface because the viscosity of the air is very small. Under wet conditions, perpendicular particle flow will be deflected into lateral flow. Compared with the V-shaped profile machined under dry conditions, due to particle deflection, the MJM has a more U-shaped machining profile.
4 Under wet conditions, due to the strong decelerating effect of the water stagnation zone near the target, the measured MJM erosion rates were slightly smaller than the erosion rates under dry conditions.
5 The sliding grinding effect under wet conditions results in an improvement in surface roughness. Particularly, for the machining of sintered materials, due to the abrasive sliding effect, the roughness of the machined surface is found to be improved more than 2.5 times.

CRediT authorship contribution statement

Yan Hu: Methodology, Investigation, Validation, Resources, Writing - original draft. **Qingwen Dai:** Methodology, Software, Validation, Resources, Writing - review & editing. **Wei Huang:** Methodology, Validation, Supervision, Writing - review & editing. **Xiaolei Wang:** Conceptualization, Supervision, Writing - review & editing, Funding acquisition.

Declaration of Competing Interest

The authors report no declarations of interest.

Acknowledgments

This work was financially supported by the National Natural Science Foundation of China (Nos. 51675268 and 51805252) and the Funding of Postgraduate Research & Practice Innovation Program of Jiangsu Province (KYCX20_0182).

References

Baba, T., Nakashima, Y., Takahashi, S., Matsubara, T., Yin, L., Nakanishi, Y., 2019. Micro slurry-jet for surface processing of dental ceramics. Biosurf. Biotribol. 5 (1), 8–12.

Balasubramaniam, R., Krishnan, J., Ramakrishnan, N., 2002. A study on the shape of the surface generated by abrasive jet machining. J. Mater. Process. Technol. 121 (1), 102–106.
Beaucamp, A., Katsuura, T., Kawara, Z., 2017. A novel ultrasonic cavitation assisted fluid jet polishing system. CIRP Ann. 66 (1), 301–304.
Bouzakis, K.D., Bouzakis, E., Skordaris, G., Makrimallakis, S., Tsouknidas, A., Katirtzoglou, G., et al., 2011. Effect of PVD films wet micro-blasting by various Al2O3 grain sizes on the wear behaviour of coated tools. Surf. Coat. Technol. 205, s128–s132.
Cao, Z.-C., Cheung, C.F., 2014. Theoretical modelling and analysis of the material removal characteristics in fluid jet polishing. Int. J. Mech. Sci. 89, 158–166.
Cao, Z.-C., Cheung, C.F., Ren, M., 2016. Modelling and characterization of surface generation in fluid jet polishing. Precis. Eng. 43, 406–417.
Coblas, D.G., Fatu, A., Maoui, A., Hajjam, M., 2015. Manufacturing textured surfaces: State of art and recent developments. Proc. Inst. Mech. Eng. Part J-J. Eng. Tribol. 229 (1), 3–29.
Denkena, B., Biermann, D., 2014. Cutting edge geometries. CIRP Ann. 63 (2), 631–653.
Freiburg, D., Aßmuth, R., Garcia Carballo, R., Biermann, D., Henneberg, J., Merklein, M., 2019. Adaption of tool surface for sheet-bulk metal forming by means of pressurized air wet abrasive jet machining. Prod. Eng. 13, 71–77.
Ghobeity, A., Crabtree, H.J., Papini, M., Spelt, J.K., 2012. Characterisation and comparison of microfluidic chips formed using abrasive jet micromachining and wet etching. J. Micromech. Microeng. 22 (2), 025014.
Haghbin, N., Spelt, J.K., Papini, M., 2015. Abrasive waterjet micro-machining of channels in metals: Comparison between machining in air and submerged in water. Int. J. Mach. Tools Manuf. 88, 108–117.
Haghbin, N., Khakpour, A., Schwartzentruber, J., Papini, M., 2019. Measurement of abrasive particle velocity and size distribution in high pressure abrasive slurry and water micro-jets using a modified dual disc anemometer. J. Mater. Process. Technol. 263, 164–175.
Hawthorne, H.M., Arsenault, B., Immarigeon, J.P., Legoux, J.G., Parameswaran, V.R., 1999. Comparison of slurry and dry erosion behaviour of some HVOF thermal sprayed coatings. Wear 225-229, 825–834.
Hu, Y., Dai, Q., Huang, W., Wang, X., 2020a. Tapered mask and its effect on the fluid flow and machining efficiency of a multiphase jet. J. Manuf. Process. 50, 467–474.
Hu, Y., Dai, Q., Huang, W., Wang, X., 2020b. Accuracy of the pattern transfer from the metal mask to the workpiece surface during multiphase jet machining. Int. J. Adv. Manuf. Technol. 106 (3–4), 1355–1364.
Huang, L., Folkes, J., Kinnell, P., Shipway, P.H., 2012. Mechanisms of damage initiation in a titanium alloy subjected to water droplet impact during ultra-high pressure plain waterjet erosion. J. Mater. Process. Technol. 212 (9), 1906–1915.
Humphrey, J.A.C., 1990. Fundamentals of fluid motion in erosion by solid particle impact. Int. J. Heat Fluid Flow 11 (3), 170–195.
Iwai, Y., Matsubara, T., Hirai, Y., Hogmark, S., 2009. Development of a new type micro slurry-jet erosion (MSE) tester for evaluation of wear properties of hard thin coatings. Lubr. Sci. 21 (6), 213–226.
Jafar, R.H.M., Hadavi, V., Spelt, J.K., Papini, M., 2016. Dust reduction in abrasive jet micro-machining using liquid films. Powder Technol. 301, 1270–1274.
Kong, M.C., Axinte, D., Voice, W., 2010. Aspects of material removal mechanism in plain waterjet milling on gamma titanium aluminide. J. Mater. Process. Technol. 210 (3), 573–584.
Kowsari, K., Nouraei, H., Samareh, B., Papini, M., Spelt, J.K., 2016. CFD-aided prediction of the shape of abrasive slurry jet micro-machined channels in sintered ceramics. Ceram. Int. 42 (6), 7030–7042.
Lehocka, D., Klich, J., Foldyna, J., Hloch, S., Krolczyk, J.B., Carach, J., et al., 2016. Copper alloys disintegration using pulsating water jet. Measurement 82, 375–383.
Leu, M.C., Meng, P., Geskin, E.S., Tismeneskiy, L., 1998. Mathematical modeling and experimental verification of stationary waterjet cleaning process. J. Manuf. Sci. Eng. 120 (3), 571–579.
Li, H.Z., Wang, J., Fan, J.M., 2009. Analysis and modelling of particle velocities in micro-abrasive air jet. Int. J. Mach. Tools Manuf. 49 (11), 850–858.
Luo, X.Y., Palumbo, J., Papini, M., Spelt, K., 2019. Aerodynamic focusing of an abrasive air jet and its effect on machining resolution. Int. J. Mach. Tools Manuf. 143, 92–106.
Maniadaki, K., Kestis, T., Bilalis, N., Antoniadis, A., 2007. A finite element-based model for pure waterjet process simulation. Int. J. Adv. Manuf. Technol. 31 (9–10), 933–940.
Mao, T.F., Yang, S.C., Tsai, F.C., Hung, J.C., Yan, B.H., 2010. Experimental investigation of abrasive jet polishing on the free-form machined surfaces of SKD61 mold steel using SiC particles. Mater. Manuf. Process. 25 (9), 965–973.
Matsumura, T., Muramatsu, T., Fueki, S., 2011. Abrasive water jet machining of glass with stagnation effect. CIRP Ann. Manuf. Technol. 60 (1), 355–358.
Messelink, W.A.C.M., Waeger, R., Wons, T., Meeder, M., Faehnle, O.W., 2005. Prepolishing and finishing of optical surfaces using fluid jet polishing. Proc. SPIE Int. Soc. Opt. Eng. 5869, 586908-586906.
Mineta, T., Takada, T., Makino, E., Kawashima, T., Shibata, T., 2009. A wet abrasive blasting process for smooth micromachining of glass by ductile-mode removal. J. Micromech. Microeng. 19 (1), 015031.
Nakanishi, Y., Nishi, N., Chikaura, H., Nakashima, Y., Miura, H., Higaki, H., et al., 2015. Textured bearing surface in artificial joints to reduce macrophage activation. Surf. Topogr. Metrol. Prop. 3 (4), 044005.
Nakanishi, Y., Baba, T., Moriyama, T., Nakashima, Y., 2017. Surface micromachining by micro slurry-jet. J. Soc. Biomech. 41 (3), 109–114.
Nakanishi, Y., Nakashima, Y., Fujiwara, Y., Komohara, Y., Takeya, M., Miura, H., et al., 2018. Influence of surface profile of Co-28Cr-6Mo alloy on wear behaviour of ultra-high molecular weight polyethylene used in artificial joint. Tribol. Int. 118, 538–546.
Nouraei, H., Wodoslawsky, A., Papini, M., Spelt, J.K., 2013. Characteristics of abrasive slurry jet micro-machining: a comparison with abrasive air jet micro-machining. J. Mater. Process. Technol. 213 (10), 1711–1724.
Old, L.T., Heitbrink, W.A., 2007. Wet abrasive blasting with a win nozzle–a case study. J. Occup. Environ. Hyg. 4 (6), D55–59.
Schreck, S., Gahr, K.H.Z., 2005. Laser-assisted structuring of ceramic and steel surfaces for improving tribological properties. Appl. Surf. Sci. 247 (1), 616–622.
Sen, B., Mia, M., Krolczyk, G.M., Mandal, U.K., Mondal, S.P., 2019. Eco-friendly cutting fluids in minimum quantity lubrication assisted machining: a review on the perception of sustainable manufacturing. Int. J. Precis. Eng. Manuf. Technol. https://doi.org/10.1007/s40684-019-00158-6.
Shi, L.P., Fang, Y., Dai, Q.W., Huang, W., Wang, X.L., 2017. Surface texturing on SiC by multiphase jet machining with microdiamond abrasives. Mater. Manuf. Process. 33 (13), 1415–1421.
Su, X., Shi, L.P., Huang, W., Wang, X.L., 2016. A multi-phase micro-abrasive jet machining technique for the surface texturing of mechanical seals. Int. J. Adv. Manuf. Technol. 86, 2047–2054.
Tsai, F.C., Ke, J.H., 2013. Abrasive jet polishing of micro-channels using compound SiC abrasives with compound additives. Int. J. Adv. Manuf. Technol. 67, 1151–1159.
Tsai, F.C., Yan, B.H., Kuan, C.Y., Huang, F.Y.A., 2008. Taguchi and experimental investigation into the optimal processing conditions for the abrasive jet polishing of SKD61 mold steel. Int. J. Mach. Tools Manuf. 48 (7), 932–945.
Tsai, F.C., Yan, B.-H., Kuan, C.-Y., Hsu, R.-T., Hung, J.-C., 2009. An investigation into superficial embedment in mirror-like machining using abrasive jet polishing. Int. J. Adv. Manuf. Technol. 43 (5–6), 500–512.
Wang, X., Kato, K., 2003. Improving the anti-seizure ability of SiC seal in water with RIE texturing. Tribol. Lett. 14 (4), 275–280.
Yan, B.H., Tsai, F.C., Sun, L.W., Hsu, R.T., 2008. Abrasive jet polishing on SKD61 mold steel using SiC coated with wax. J. Mater. Process. Technol. 208 (1–3), 318–329.
Yu, H., Huang, W., Wang, X., 2013. Dimple patterns design for different circumstances. Lubr. Sci. 25 (2), 67–78.
Yuan, S., Huang, W., Wang, X., 2011. Orientation effects of micro-grooves on sliding surfaces. Tribol. Int. 44 (9), 1047–1054.
Zhang, T., 2013. Influence of size effect on burr formation in micro cutting. Int. J. Adv. Manuf. Technol. 68 (9–12), 1911–1917.
Zhang, X., Zhou, C., Jiang, L., Rui, Guo, 2017. Influence of process parameters on abrasive particle motion characteristics in abrasive water jet descaling. Int. J. Adv. Manuf. Technol. 90 (9–12), 2741–2749.